Research Square

Preprints are preliminary reports that have not undergone peer review.
They should not be considered conclusive, used to inform clinical practice,
or referenced by the media as validated information.

Electrical Modulus and Impedance Analysis of Sintered Fly Ash

Himansu Sahoo
Department of Metallurgical and Materials Engineering, IGIT, Sarang Dhenkanal, Odisha, 759146
Prafulla Kumar Mallik
prafulla.mallik@gmail.com

Department of Metallurgical and Materials Engineering, IGIT, Sarang Dhenkanal, Odisha, 759146
Kashinath Barik
Department of Chemical Engineering, IGIT, Sarang Dhenkanal, Odisha, 759146

Research Article

Keywords: Sintered Fly ash, impedance properties, electric modulus, microstructure, powder metallurgy

Posted Date: June 24th, 2026

DOI: https://doi.org/10.21203/rs.3.rs-10125551/v1

License: This work is licensed under a Creative Commons Attribution 4.0 International License.
Read Full License

Additional Declarations: The authors declare no competing interests.

Electrical Modulus and Impedance Analysis of Sintered Fly Ash

H Sahoo[1], P K Mallik[1], K Barik[2]
[1]Department of Metallurgical and Materials Engineering, IGIT, Sarang Dhenkanal, Odisha, 759146
[2]Department of Chemical Engineering, IGIT, Sarang Dhenkanal, Odisha, 759146

*Corresponding author: prafulla.mallik@igitsarang.ac.in

Abstract

Over the last few decades, the most effective and profitable use of fly ash has been a topic of research in the scientific community. However, research results have yet to show interest in the electrical properties of fly ash. This study utilized a novel powder metallurgy method to investigate the electrical impedance and modulus properties of sintered fly ash. The correlation between the microstructural and electrical impedance properties was determined by X-ray diffraction (XRD), Scanning Electron Microscope (SEM), and Impedance analysis. The effects of bentonite addition on the microstructure, electric modulus, and impedance properties of the sintered fly ash were studied. As a result, sintered fly ash exhibits a better microstructure and frequency- and temperature-dependent electric modulus properties. It has been suggested that sintered fly ash can be utilized in electronic packaging and EMI shielding applications.

Keywords: Sintered Fly ash; impedance properties; electric modulus; microstructure; powder metallurgy

INTRODUCTION

Over the years, the use of fly ash has increased significantly, and its production has grown in tandem with the number of thermal power stations. Therefore, alternative uses of fly ash as a value-added product are required [1]. The safe and beneficial utilization of fly ash has been a topic of research in the scientific community, including construction materials [2], wear-resistant ceramic liners [3,4], ceramic glass [5], composites [6, 7], and ceramic tile [8-10]. In other words, various physical, chemical, and mechanical properties of FA have been studied. However, there are limited studies on functional properties, such as dielectric and electrical properties [11-17]. Furthermore, additional studies are needed on the functional properties of sintered fly ash, including its electrical impedance and modulus.

In this study, a novel powder metallurgy method was used to investigate the effect of bentonite addition on the dielectric (dielectric constant and dielectric loss) and electrical (impedance and modulus) properties of fly ash sintered at different frequencies and temperatures. Impedance spectroscopy allowed us to evaluate and distinguish the roles of various components, including grains and grain boundaries, in the overall electrical behavior of sintered fly ash. The electric modulus

technique provides insights into the bulk response, enabling separation of local defect behaviors, such as porosity, from electrode effects. This study aims to examine the bulk and interface phenomena over a wide frequency range at selected temperatures to determine the relaxation times and amplitudes of various processes occurring in sintered fly ash under an electric field. It is also important to note that analyzing the complex impedance spectra can reveal multiple physical parameters and key properties that influence the performance of sintered fly ash as a value-added product. X-ray Diffraction (XRD), Scanning Electron Microscope (SEM), and impedance analyzers were used to investigate the relationship between the microstructure and electrical impedance properties of the sintered fly ash.

EXPERIMENTAL PROCEDURES

2.1. Sample preparation

Fly ash was collected from NALCO, Angul, Odisha. After that, it was oven-dried at 100 °C for 24 hours. Bentonite powder was purchased from Loba Chemical (Shanghai, China). The chemical compositions of fly ash and bentonite are presented in Table 1.

Fly ash was mixed with bentonite at a 10% weight ratio and ground in a ball mill for 5 h. Then, the fly ash was dried in a heating oven at 100 °C for 6 hours to remove moisture. The pellets were prepared using a hydraulic compaction machine at 220 MPa for 20 seconds. Green pellets were sintered at 1100 °C for 2 hours. These sintered samples were polished and characterized using various techniques.

2.3. Characterization of sintered fly ash

X-ray diffraction (XRD) experiments were performed to determine the minerals and crystalline phases of the FA, bentonite powders, and sintered fly ash using a Bruker X-ray diffractometer (CuKα radiation, $\lambda = 0.154$ nm). The powder and sintered samples were scanned over a 2θ range of 10° to 100° at a scanning rate of 2°/min.

The morphologies and compositions of the FA, bentonite powders, and sintered fly ash were analyzed using field-emission scanning electron microscopy (FESEM; Carl Zeiss Supra 40) equipped with an Energy-dispersive X-ray spectroscopy (EDX) system, which enabled qualitative and quantitative analysis. The operating voltage was maintained at 20 kV.

For the impedance and modulus measurements, the polished samples were coated with silver paste and dried to serve as the sample electrode. The capacitance, real part of complex permittivity (ε'), the imaginary part of complex permittivity (ε'), and dielectric loss were measured as a function of frequency (100Hz-1MHz) and temperature from 30 °C to 210 °C using a Precision Impedance analyzer (Wayne Kerr, 6500b, UK). The samples were then heated at a rate of 2 °C/min. In this study, the AC electric signal applied to the samples was 1V. The complex impedance (Z^*) and modulus (M^*) were calculated using the following formulae:

The complex permittivity data were calculated using the real and imaginary parts of complex permittivity (ε^*). The following formula

$$\varepsilon^* = \varepsilon' - j\varepsilon'' \quad (1)$$

Impedance spectroscopy data are calculated using the following formula

$$Z^* = Z' + jZ'' \quad (2)$$

The real and imaginary parts of the complex electrical impedance were calculated using the following expressions:

$$Z' = \frac{1}{2\pi f C_\circ}\left[\frac{\varepsilon''}{\varepsilon'^2 + \varepsilon''^2}\right] \quad (3)$$

$$Z'' = \frac{1}{2\pi f C_\circ}\left[\frac{\varepsilon'}{\varepsilon'^2 + \varepsilon''^2}\right] \quad (4)$$

Where $\varepsilon^*$is relative permittivity; $Z^*$is the complex impedance; f=frequency; $C_\circ$ is the geometrical capacitance; j = √-1; ε_o is the permittivity of vacuum (8.854×10−12 F/m).

The electrical modulus can be expressed using the relation

$$M^* = M' + jM'' \quad (5)$$

The real (M')and imaginary (M'') parts of the complex electrical modulus (M*) were calculated using the following expressions:

$$M' = \frac{\varepsilon'}{\varepsilon'^2 + \varepsilon''^2} \quad (6)$$

$$M'' = \frac{\varepsilon''}{\varepsilon'^2 + \varepsilon''^2} \quad (7)$$

where are the real (ε': relative permittivity) and imaginary parts (ε'': dielectric loss) of the complex permittivity, respectively.

3. RESULTS AND DISCUSSION

3.1. Composition and microstructure analysis
XRF results of raw fly ash and bentonite powder are shown in Table 1

Table 1: Chemical analysis of raw fly ash powders

Chemical Composition	Fly ash wt.%	Bentonite wt.%
Al_2O_3	24.92	25.8
SiO_2	59.42	46.80
CaO	0.76	3.37
Fe_2O_3	8.16	6.006
TiO_2	4.03	-
Na_2O	0.142	3.87
K_2O	1.29	0.32
MgO	0.59	2.09
P_2O_5	0.33	-
SO_3	0.36	-
Fe	-	4.2
LOI	-	8.65

3.2. XRD analysis

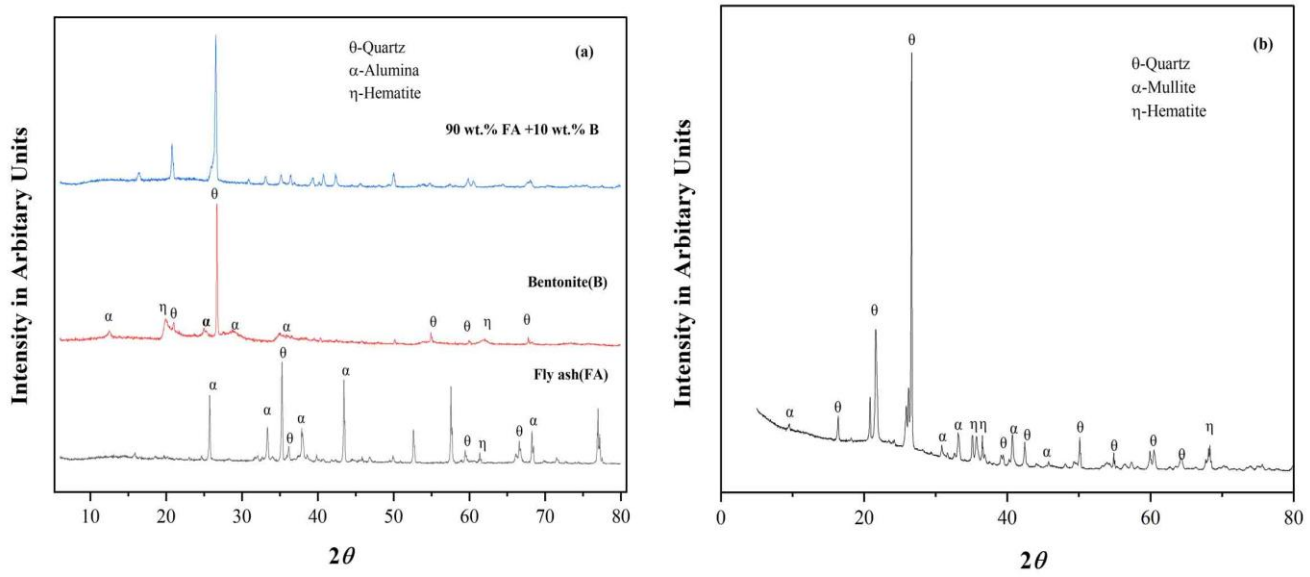


Fig.1. (a) XRD analysis of powder; (b) XRD analysis of sintered fly ash at 1100 °C.

XRD analysis of raw fly ash powders, including bentonite, fly ash, and fly ash with 10 wt. %, is shown in Figure 1 (a) and (b). The bentonite percentage exhibited a peak, indicating crystallinity. However, Figure 1(b) shows that the sintered fly ash at 1100 °C for 2 h exhibits strong peaks corresponding to quartz and weaker peaks corresponding to mullite and hematite.

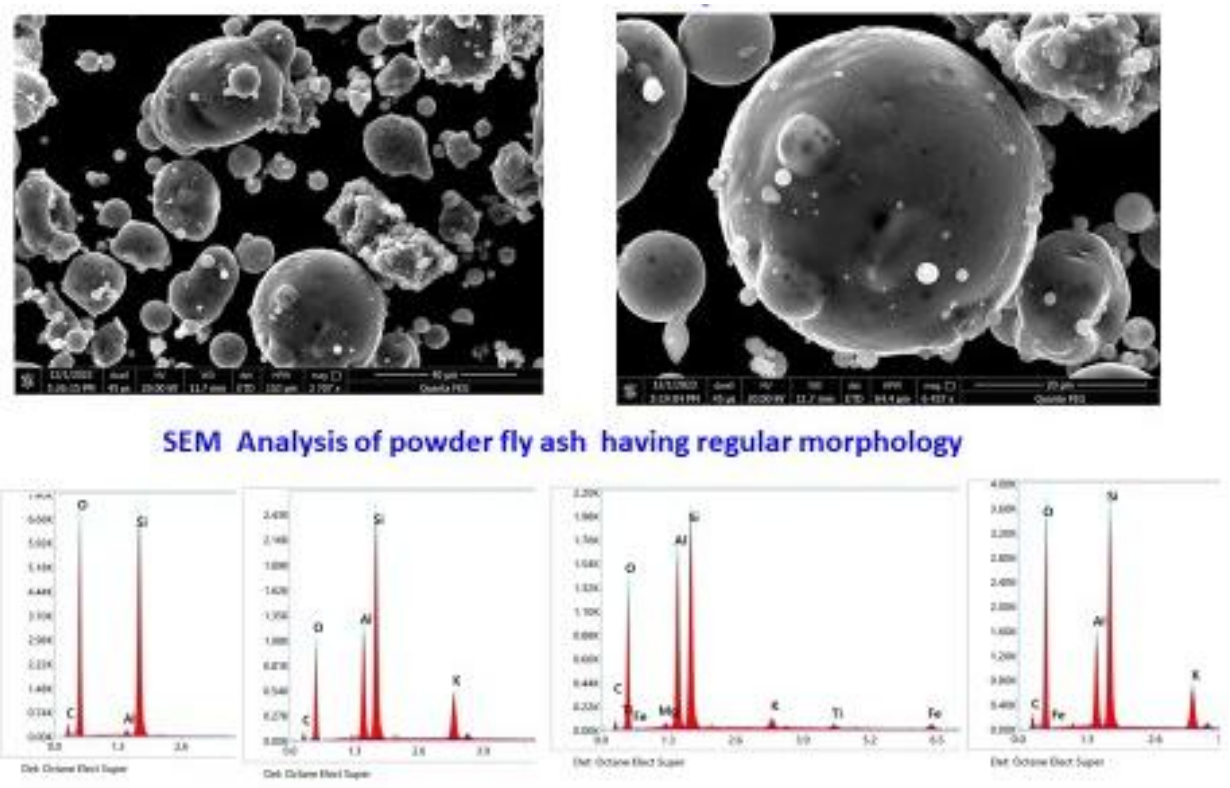


Figure 2 (a) shows the Morphology and the EDX spectrum of the fly ash raw powders.

The EDX spectrum of the raw fly ash powders shown in Figure 2 reveals the presence of Fe, Al-Si, C, O, Na, Mg, Ca, and Ti in the sample, as listed in Table 1. Figure 2 shows the morphology of the spherical particles mixed with agglomerated particles.

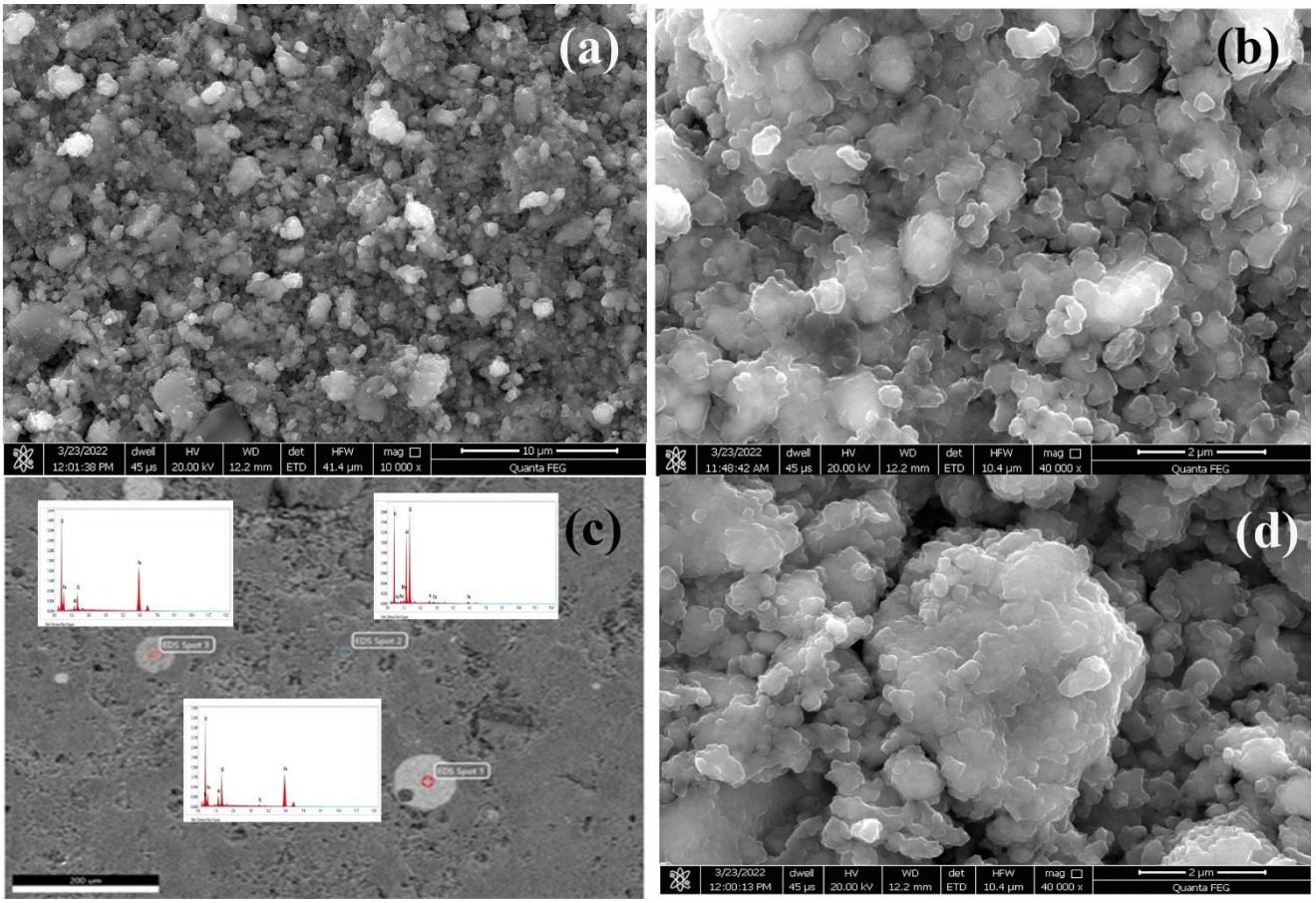


Figure 3. (a) SEM image of sintered fly ash at low magnification; (b) SEM image of sintered fly ash at high magnification; (c) EDX of the sintered fly ash; (d) showing the agglomeration of fly ash powders during sintering.

Figure 3(a) shows that the microstructure of the sintered fly ash consisted of individual grains and agglomerates dispersed over the sample surface. In Figures 3(b) and 3 (d), the higher-magnification image of the sintered fly ash shows interconnected grains and agglomerates. Deep porosities were observed in the microstructure, resulting in a reduced sample density.

3.3. Dielectric Analysis

Figure 4(a) shows the results ε′ as a function of the frequency at various temperatures. It can be observed that the increased with increasing temperature (i.e., 30–210 °C) and then decreased slowly with increasing frequency. At low frequencies, the space-charge and orientation-polarization carriers respond more quickly to the externally applied electric field, resulting in a higher value of ε′. At higher frequencies, these charge carriers cannot keep up with the rapid changes in the frequency of the applied electric field, which causes a decrease in ε′. Space charge and orientation polarization occur in relation to the microstructure of sintered fly ash at frequencies ranging from 1 kHz to 1 MHz.

The microstructure comprised grains, such as mullite and quartz, and grain boundaries, including an amorphous aluminosilicate glass phase. The permanent dipoles align with the applied electric field at the defect sites in the sintered fly ash, such as the porosity. Orientation polarization and space-charge accumulation at the grain boundaries are responsible for the higher values of at low frequencies. Furthermore, the values of ε′ decrease at higher frequencies because interfacial polarization does not respond instantly as the frequency of the alternating electric field increases. The increase in temperature is attributed to the contribution of free charge carriers to polarization, as shown in Figure 4(b). At low temperatures, polarization is weak because the dipoles cannot rotate sufficiently quickly to follow the oscillating electric field. Higher temperatures provide sufficient thermal energy to bind charge carriers, such as those in SiO_2, thereby enhancing the polarization and increasing ε′ at various frequencies.

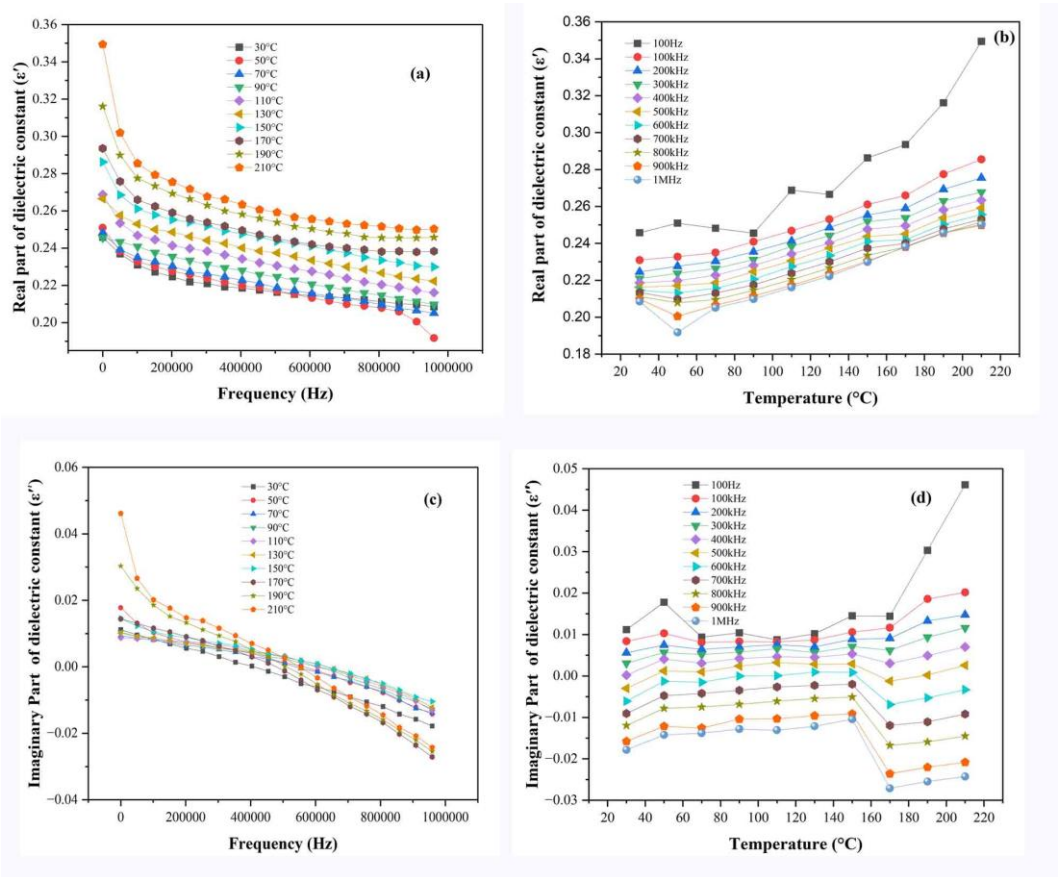


Figure 4 (a) and (b) show the results ε″with varying frequencies and temperatures, and (c) and (d) show the results ε″with varying frequencies and temperatures of the sintered fly ash.

Figure 4(c) shows ε″ that varies with the frequency at various temperatures. It can be seen that the decrease in ε″ with increasing frequency might be due to the higher conductivity of the material. The sharp rise in ε″ at higher temperatures in the low-frequency range could be caused by space charge polarization. The variation in ε″ with frequency also indicates the presence of a relaxation process, that shifts to a higher frequency range at high temperatures, highlighting the influence of AC conductivity. As a result, the relaxation time decreased with increasing charge-carrier mobility in the low-frequency range at low temperatures, revealing the impact of DC conductivity. In contrast, the

ε″ as it varies with temperature at different frequencies appears as two relaxation peaks at low temperatures of 50 °C and high temperatures of 120 °C. Furthermore, ε″ increased with increasing temperatures.

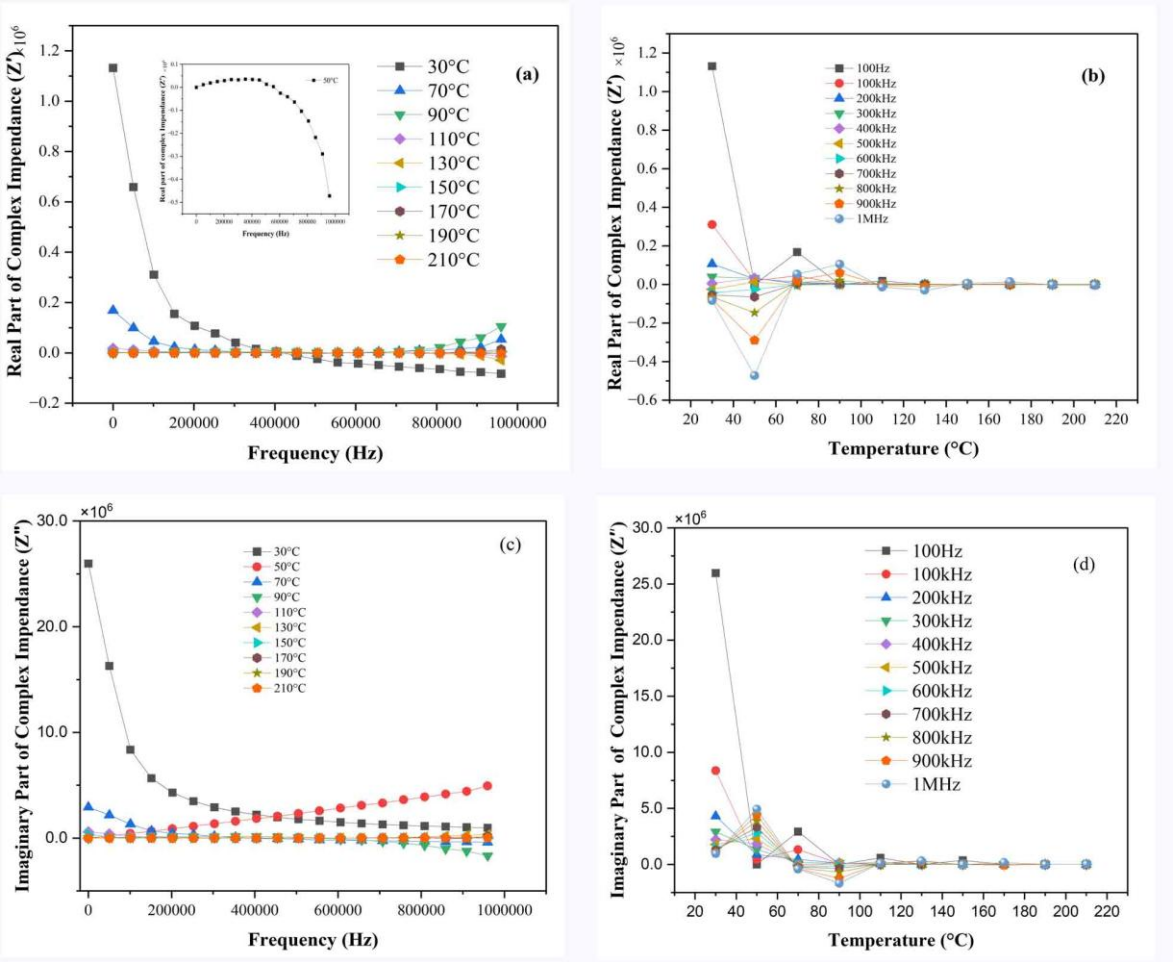


Figure 5: (a) and (b) show Z′ with varying frequency and temperature, and (c) and (d) show Z″ with varying frequency and temperature of the sintered fly ash.

In Figure 5(a), Z' is displayed as a function of frequency and temperature. A decrease in Z was observed with increasing temperature at low frequencies, as shown in Figure 5(b). This behavior indicates that Z ′of sintered fly ash is associated with a capacitive reactance, which opposes the mobility of charge carriers under the applied frequency of the electric field. It was also observed that the curves converged into a single line at high frequencies, regardless of temperature, demonstrating the space-charge-dependent behavior of the material [18]. Indeed, the accumulated charge carriers near the phase boundaries have sufficient energy to overcome this barrier, resulting in increased conductivity and decreased impedance.

The Z″ values as a function of the frequency at different temperatures are shown in Figure 5(c). It can be observed that a single impedance plot appears at 50 °C and shifts toward higher frequencies as the frequency increases. This indicates that the electrical reactance of the sintered fly ash material was activated at this temperature, opposing the flow of the mobile charge carrier under the applied electric field. Additionally, the maximum value of Z" decreased rapidly with temperature, clearly

demonstrating the strong temperature dependence of the resistance of the sintered fly ash as shown in Figure 5(d). It was also observed that at 120 °C, all curves converged into a single curve, regardless of temperature, demonstrating the space charge-dependent behavior of the material.

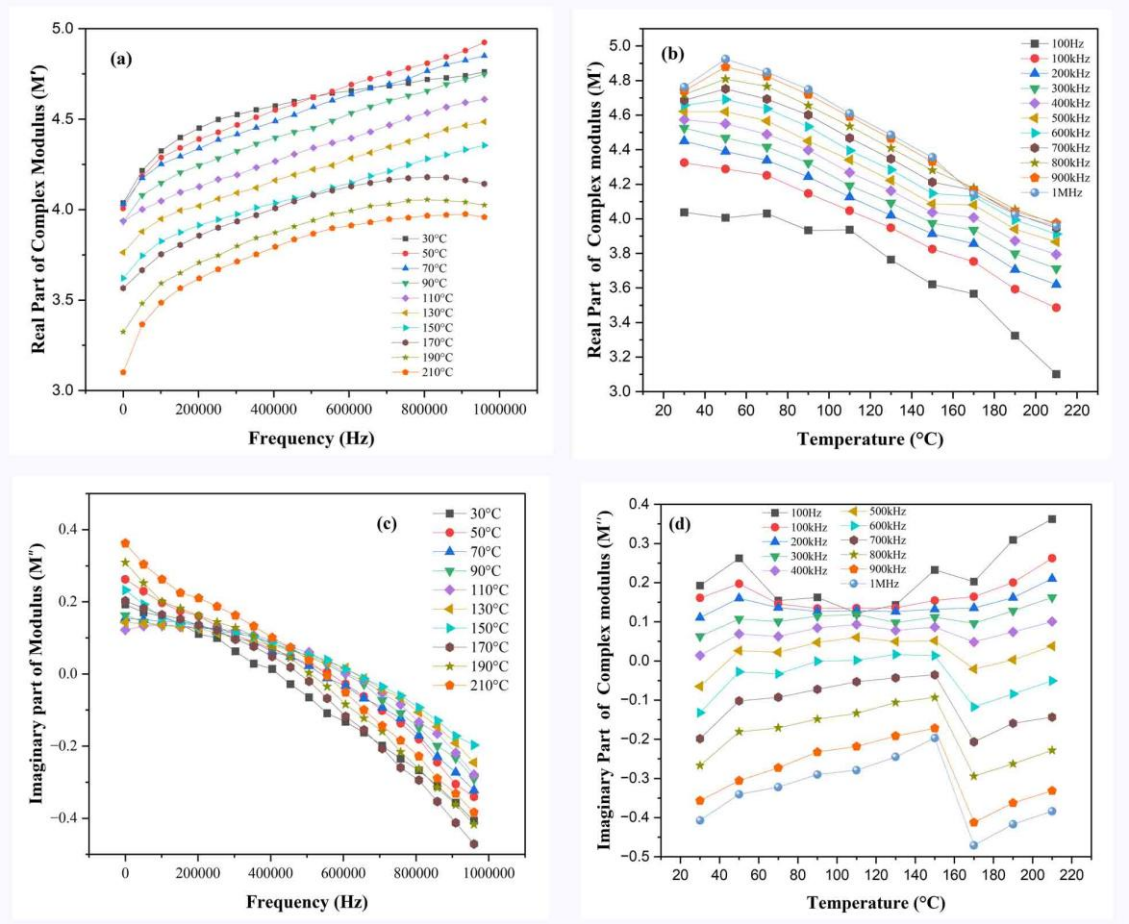


Figure 6. (a) and (b) show M′ with varying frequency and temperature, and (c) and (d) show M″ with varying frequency and temperature of the sintered fly ash.

The electric modulus shows how the electric field relaxes in sintered fly ash, representing the actual dielectric relaxation process. M* is inversely related to the permittivity of the material and is given as $M^* = 1/\varepsilon^*$. This offers an alternative approach for analyzing the electrical response of sintered fly ash grains and the effects of grain boundaries at high temperatures. The complex electric modulus is frequently discussed in conjunction with permittivity and impedance to understand how grain boundaries affect the relaxation process and to investigate long-range conduction and localized dielectric relaxation at the microscopic level [19-25]. Figure 6 (a) shows the frequency dependence of M′ over the temperature range of 30 °C to 210 °C. It was observed that as the applied electric field increased, the real part of the complex modulus decreased with increasing temperature. Additionally, at low frequencies and temperatures, the M′ value for the sintered fly ash was higher than that at high frequencies and temperatures. The relaxation peaks occur at higher frequencies as the temperature increases because of the accumulation of free charges at the grain-grain and grain-boundary interfaces in the sintered fly ash. Consequently, the increased charge-carrier mobility in the sintered

fly ash shortened the relaxation time, and the peaks shifted to higher frequencies as the temperature increased. This suggests that the hopping mechanism of the mobile charge carriers is a thermally activated process.

Figure 6(b) shows temperature-dependent M′ values at various frequencies. The real part of the electrical modulus decreases with increasing temperature. At lower temperatures and frequencies, the M′ value for the sintered fly ash was lower than that at higher temperatures and frequencies. The relaxation peaks occur at lower temperatures as the frequency increases, owing to the accumulation of free charges and space charges at the grain-grain boundary and grain boundary regions of the sintered fly ash. As the temperature increases, the increase in charge-carrier mobility results in longer relaxation times at higher frequencies, indicating that dielectric relaxation is a thermally activated process primarily governed by charge-carrier hopping.

Figure 6 (c) shows the frequency dependence of M″ at various temperatures. It is clear that at low frequencies and high temperatures, M″ for sintered fly ash is higher than that at higher frequencies and lower temperatures. Additionally, at different frequencies, the temperature-dependent M″ shows that M″ is lower at higher temperatures and frequencies, as shown in Figure 6(d). Figures 6(c) and 6(d) show that the M″ versus frequency and temperature-dependent curves exhibit peaks at low and high frequencies, respectively, or vice versa. As a result, the peaks shift to higher-frequency regions and increase in temperature owing to the accumulation of free charge at the grain boundaries of the sintered fly ash. Therefore, the increase in the mobility of the charge carriers reduces the dielectric relaxation time, which is a thermally activated process dominated by the hopping mechanism of charge carriers in sintered fly ash.

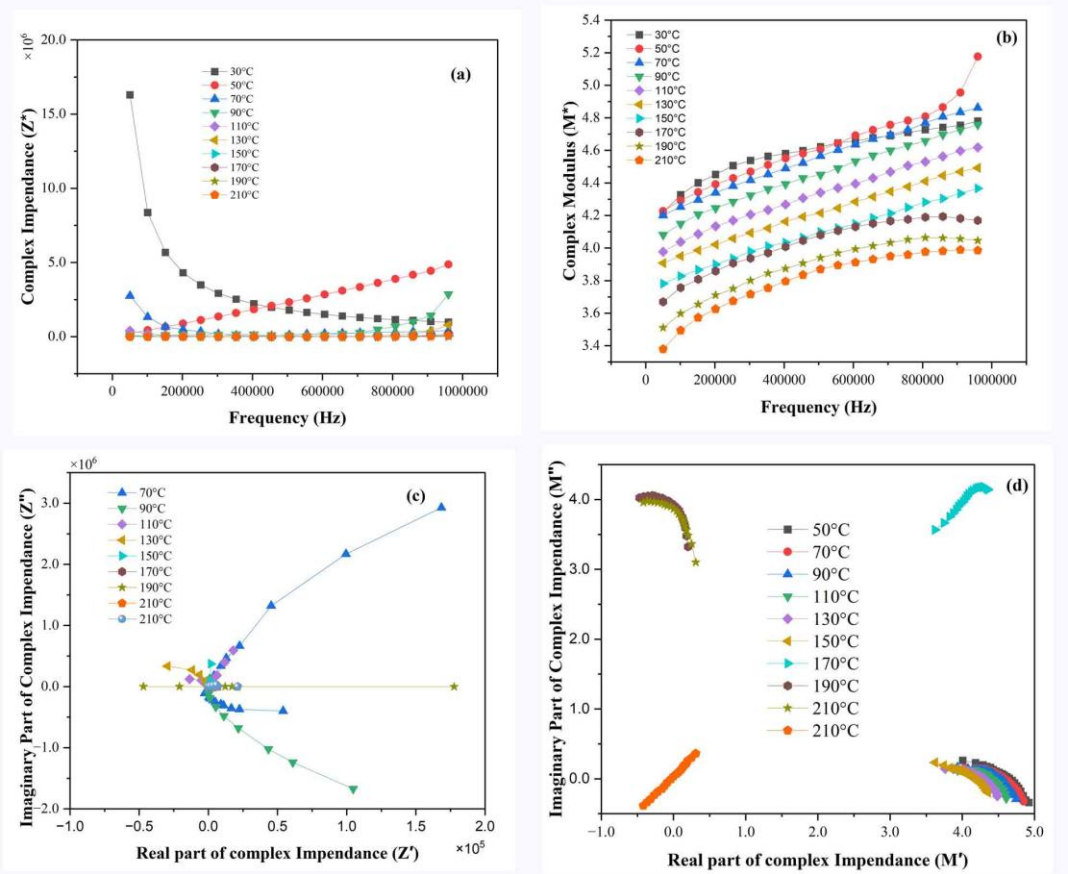


Figure 7. (a) and (b) frequency-dependent electrical impedance and modulus, (c) Z″ versus Z′, and (d) M″ versus M′ of sintered fly ash in the temperature range of 30°C to 210°C and frequency from 100Hz to 1MHz.

Figure 7(a) shows how Z* varies with the frequency at different temperatures. At 30 °C, the complex impedance decreases with increasing frequency, whereas at 50 °C, it increases with frequency. At other temperatures, the complex impedance of sintered fly ash remained constant over a wide frequency range. This clearly indicates that the impedance of the grains and grain boundaries in the sintered fly ash remained stable at higher frequencies and temperatures. This stability was due to the presence of mullite, a reactive amorphous aluminosilicate glass phase, and quartz in the sintered fly ash, which caused the formation of various barium-containing phases. Based on this, it can be concluded that sintered fly ash can serve as an insulator for high-power transmission.

Figure 7(b) shows the dependence of M* on the frequency at different temperatures. It was observed that M* increases with frequency across a range of temperatures. Additionally, the dielectric relaxation peaks of the sintered fly ash appeared at high temperatures and frequencies. At medium temperatures, the relaxation time increased from 30°C to 150°C, shifting the peak toward higher frequencies. Mobile charge carriers are activated by the frequency of an applied electric field within a specific temperature range. Further increasing the temperature and frequency causes a sudden release of accumulated charge carriers at the grain boundaries. Consequently, a relaxation peak appeared at higher frequencies and temperatures.

Figure 7(c) shows the Nyquist plots of the Z″ versus Z′ at different frequencies (100 Hz to 1 MHz) and temperatures (30°C to 210°C). This plot enabled us to distinguish between the real and imaginary components of the impedance parameters, providing insight into the relationship between the microstructure and the electrical properties of the sintered fly ash sample. The microstructure of the sintered fly ash comprises grains (such as mullite and quartz) and grain boundary properties resulting from the amorphous aluminosilicate glass phase, which exhibits different time constants at high temperatures, leading to a single semicircle and upper and lower planes at a particular value of Z″. The appearance of single semicircles in the lower and upper planes suggests the presence of both grain and grain boundary effects in the polycrystalline sintered fly ash samples.

Figure 7(d) shows the frequency-dependent electrical modulus plane plots of sintered fly ash, displaying M″ versus M′ curves over a temperature range of 30 °C to 210 °C. The intercept on the real axis indicates the capacitance related to either the grain or the grain boundary. Semicircle curves appeared in the modulus plane plot of sintered fly ash at both low and high frequencies, indicating four relaxation processes at different temperatures. The small semicircle at low frequency and high temperature is associated with weak grain boundary effects rather than dominant grain effects. The larger semicircle curves at high and low temperatures represent the bulk or grain response. A deviation from the typical semicircle shape of the modulus curve in the sintered fly ash occurs at 210 °C in the low-frequency region and at 170 °C in the high-frequency region. However, the semicircular curve for the sintered fly ash sample appeared only at other frequencies.

CONCLUSION

Fly ash mixed with 10 wt% bentonite was successfully prepared using powder metallurgy. The XRD analysis revealed strong quartz peaks and weaker mullite and hematite peaks. SEM analysis revealed deep porosities in the microstructure, which decreased the density of sintered fly ash. The Nyquist plot analysis revealed an inverted semicircle, attributed to differences in composition and defects. Cole-Cole plots of electric moduli analysis indicate that the four-quadrant curve suggests the contribution of four types of relaxation times: quartz, mullite, hematite, and grain boundaries, as well as porosity.

Acknowledgements

The authors acknowledge the support of the Science and Engineering Research Board (SERB), Department of Science and Technology (DST), Ministry of Science and Technology, and AICTE, Government of India, for the facility support. Thank you, Director, IGIT, and Sarang, for providing the facility.

Conflicts of interest

The authors have declared that no competing interests exist.

Data access statement

All relevant data are within the paper and its Supporting Information files.

REFERENCES

1. Iyer, R. S., and J. A. Scott. "Power station fly ash—a review of value-added utilization outside of the construction industry." Resources, conservation and recycling 31.3 (2001): 217-228.

2. S. S. Alterary, N. H. Marei, Fly Ash properties, characterization, and applications, Journal of King Saud University – Science, 33 (2021) 101536-44.

3. S. K. Malviya, B. Chatterjee, K. K. Singh, Fly Ash Utilization for Value Added Products, (1999)59-67.

4. S. K. Das, K. N. Gupta, K. C. Roy, and B. K. Mitra, Proceedings of 8th CIMTEC World Ceramic Congress, held in Florence, Italy, (1995)2403–2411.

5. R. Cioffi, P. Pernice, A. Aronne, M. Catauzo, G. Quattroni, Effect of size of fly ash particle on enhancement of mullite content and glass formation. J. Eu. Cer.Soc., 13(1994)143-148.

6. P. K. Rohatagi, Low-Cost, Fly-Ash-Containing Aluminum-Matrix Composites J.O.M., (1994) 55–59.

7. Abhijit Dey and Krishna Murari Pandey, Characterization of fly ash and its Reinforcement effect on Metal Matrix Composites, Rev.Adv. Mater. Sci., 44 (2016) 168-181.

8. S. K. Das, S. Kumar, K. K. Singh, P. R. Rao, Proceedings of the National Seminar on RVBIS, held in Ghatsila, India. IIM, (1996) 7–10.

9. S. Kumar, K. K. Singh, P. R. Rao, Effects of fly ash additions on the mechanical and other properties of porcelainized stoneware tiles., J.Mat.Sci., 36(2001) 5917–5922.

10. Shah, H. M. and Maiti, K. N., Development of Glazed Wall Tiles through Optimal Utilization of Fly Ash, Trans. Ind. Ceram. Soc., 60(3) (2001)145–149.

11. S. C. Raghavendra, R. L. Raibagkar and A. B. Kulkarni, Dielectric properties of fly ash, Bull. Mater. Sci., 25(2002)37–39.

12. B. Cumpston, F. Shadman, S. Risbud, Utilization of coal-ash minerals for technological ceramics. J. Mater. Sci., 27 (1992), pp. 1781-1784.

13. S. Hanjitsuwan1, P. Chindaprasirt, K. Pimraksa, Electrical conductivity and dielectric property of fly ash geopolymer composites. Int. J.of Minerals, Metallurgy and Materials,18(2011) 94-99.

14. S. Joshia, S.K. Ubaleaand S.J. Dhobleb, to study of electrical resistivity of fly ash composite, JETIR,7(2020)1050-1058.

15. M.K. Panigrahi, Investigation of Structural, Morphological, Resistivity of Novel Electrical Insulator: Industrial Wastes. Bull. Sci. Res. 3(1) (2021) 51-58.

16. M.K. Panigrahi, Investigation of Structures of Sintered Processed Fly Ash Materials: Resources of Industrial Wastes. Bull. Sci. Res, 4(1) (2022) 1-10.

17. Ayeni, J. O., Ma, S., Wang, X., & Hou, X. (2022). Fabrication method, dielectric properties, and electromagnetic absorption performance of high alumina fly ash-based ceramic composites. Ceramics International 48 (2022) 21268–21282.

18. Sahoo, H., Mallik, P. K., & Barik, K. (2024). Microstructural and functional characterization of sintered fly ash. Engineering Research Express, 6(3), 035412.

19. V. F. Lvovich, Impedance Spectroscopy, Applications to Electrochemical and Dielectric Phenomena, John Wiley & Sons, Inc., 2012.

20. N. Bonanos, B. C. H. Steele, and E. P. Butler, Impedanc Spectroscopy Theory, Experiment, and Applications, John Wiley & Sons, New Jersey, 2005.

21. P. C. Sati, M. Kumar and S. Chhoker, Low temperature ferromagnetic ordering and dielectric properties of Bi1-xDyxFeO3 ceramics. Ceram. Int., 2015, 41, 3227–3236.

22. P. Gogoi, P. Srinivas, P. Sharma and D. Pamu, Optical, Dielectric Characterization and Impedance spectroscopy of Ni-substituted $MgTiO_3$ Thin Films. J. Electron.Mater., 2016, 45, 899.

23. Z. Cao, X. Liu, W. He, X. Ruan, Y. Gao and J. Liu, Temperature dependence of spin-polarized absorption spectra and optical properties of CdSe/BeTe quantum dots. Phys. B, 2015, 477, 8–13.

24. I. Coondoo, N. Panwar, A. Tomar, A. K. Jha and S. K. Agarwal, Impedance Spectroscopy and conductivity studied in $SrBi_2$ $(Ta_{1-x}W_x)_2O_9$ Ferroelectric ceramic. Phys. B, 2012, 407, 4712–4720.

25. R. Lefi, F. Ben Nasr, H. Hrichi and H. Guermazi, Optical and electrical properties and characterization of $(C_2H_5NH_3)_2CdCl_4$ compound. Optik, 2016, 127, 5534–5541.